NANO LETTERS

Letter

pubs.acs.org/NanoLett

Excitonic Lasing in Solution-Processed Subwavelength Nanosphere Assemblies

Kannatassen Appavoo,[†] Xiaoze Liu,[‡] Vinod Menon,[‡] and Matthew Y. Sfeir*[,†]

[†]Center for Functional Nanomaterials, Brookhaven National Laboratory, Upton, New York 11973, United States

[‡]Department of Physics, City College of New York, New York, New York 10031, United States

Supporting Information

ABSTRACT: Lasing in solution-processed nanomaterials has gained significant interest because of the potential for low-cost integrated photonic devices. Still, a key challenge is to utilize a comprehensive knowledge of the system's spectral and temporal dynamics to design low-threshold lasing devices. Here, we demonstrate intrinsic lasing (without external cavity) at low-threshold in an ultrathin film of coupled, highly crystalline nanospheres with overall thickness on the order of $\sim\lambda/4$. The cavity-free geometry consists of ~35 nm zinc oxide nanospheres that collectively localize the in-plane emissive light fields while minimizing scattering losses, resulting in excitonic lasing with fluence thresholds at least an order of magnitude lower than previous UV-blue random and quantum-dot lasers (<75 μJ/cm^2). Fluence-dependent effects, as quantified by subpicosecond transient spectroscopy, highlight the role of phonon-mediated processes in excitonic lasing. Subpicosecond evolution of distinct lasing modes, together with three-dimensional electromagnetic simulations, indicate a random lasing process, which is in violation of the commonly cited criteria of strong scattering from individual nanostructures and an optically thick sample. Subsequently, an electron−hole plasma mechanism is observed with increased fluence. These results suggest that coupled nanostructures with high crystallinity, fabricated by low-cost solution-processing methods, can function as viable building blocks for high-performance optoelectronics devices.

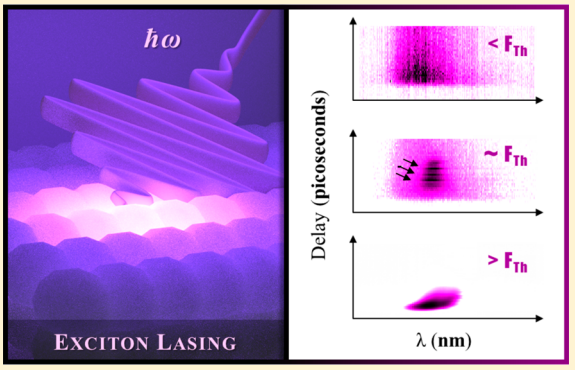

KEYWORDS: *Cavity-free, room-temperature random lasing, solution-processed film, ultrafast dynamics, electron−phonon coupling, near-field enhancement*

For integrated photonic applications, it is necessary to develop low cost, high-efficiency light amplification processes. While various strategies have been explored over the past decade,[1−3] two distinct schemes have been investigated for disordered media, amplified spontaneous emission in thin films of nanometer-sized quantum dot nanostructures (QD-ASE) and random lasing in larger, micron-sized structures. Each strategy has critical inherent drawbacks that have so far limited their practical use. In QD-ASE devices, weakly scattering nanometer-sized particles allow for the long optical path lengths necessary to achieve optical gain. As a result, the incoherent emission profile is derived solely from the gain curve of the medium, which is tunable via the size dependent optical properties of quantum dots. However, relatively large critical volumes are required for light amplification in these systems and their efficiency is highly sensitive to the initial excitonic states that are excited and their relaxation dynamics.[4−7] As a result, complex band engineering strategies, for example, core/shell nanostructures, are necessary to reduce losses via nonradiative Auger recombination and reabsorption.[1,8−11] In contrast, in random lasers, constructive light interference via multiple scattering leads to the evolution of distinct modes in the lasing spectrum. Here, materials are typically chosen to provide both scattering and gain functionality, either by mixing nonresonant scatterers with a gain medium such as a laser dye[12−14] or by using bifunctional materials that provide both.[15−17] While considerable work has been done to tune the particle size to optimize resonant scattering at the band-edge emission wavelength,[18−20] losses remain high, leading to lasing thresholds in the few mJ/cm^2 range.[18] As a result of these challenges, current QD-ASE and random lasing schemes do not offer the ideal device characteristics of both small critical dimensions and low lasing threshold.

In this letter, we demonstrate the emergence of short-lived collective emission modes through a low threshold, excitonic lasing process in subwavelength thin films of ZnO nanospheres (average diameter of ~35 nm) with weak individual scattering properties. In contrast to previous studies that have focused mainly on maximizing the scattering efficiency of individual nanostructures at the lasing wavelength with predicted optimal sizes of ~260 nm,[18−20] here we show that efficient, low-threshold lasing is achieved by using much smaller, highly

Received: December 27, 2015
Revised: January 28, 2016
Published: February 3, 2016

DOI: 10.1021/acs.nanolett.5b05274
Nano Lett. 2016, 16, 2004−2010

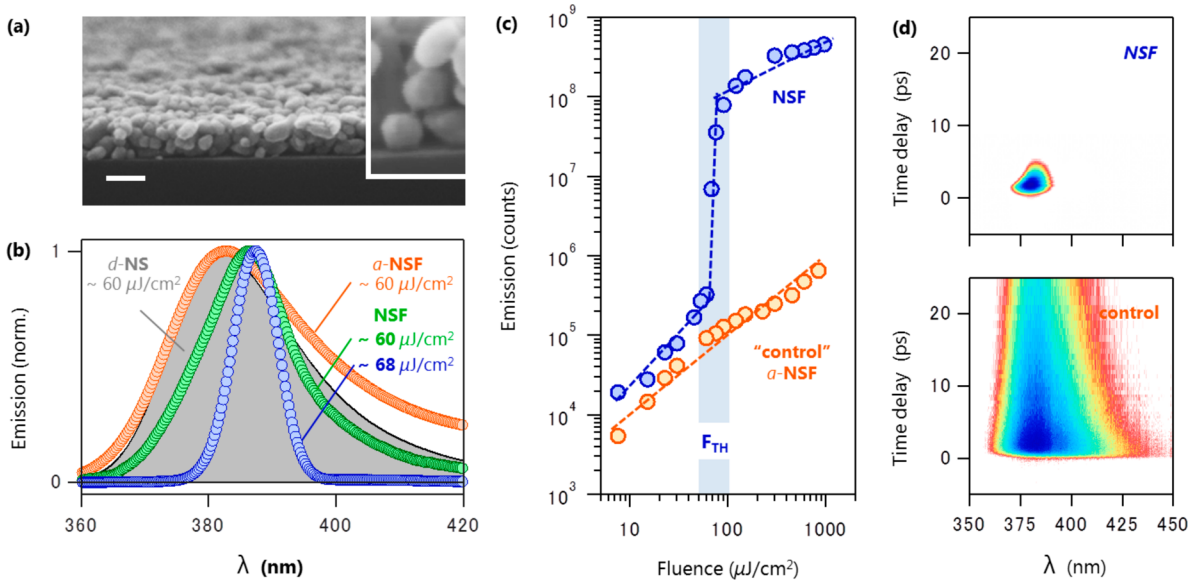

Figure 1. Coupling effect of nanostructures on emission intensity. (a) Scanning electron micrographs of thin-film coupled nanostructures (NSF) exhibiting lasing. Scale bar is 100 nm and nanospheres are ~35 nm in diameter. (b) Normalized emission spectra for pristine NSF near threshold (60 μJ/cm^2, green) and at threshold (68 μJ/cm^2, blue), along with one sample that has been annealed for a short duration (a-NSF, orange) and when nanospheres are dispersed in ethanol (d-NS, shaded gray). Note that the broader line width for the anneal sample is due to emission from interfacial defect states that contribute to the lower energy tail of the band-edge emission. (c) Peak emission intensity at the band-edge as a function of pump fluence for a pristine film of nanospheres (NSF, blue) and one annealed for a short duration (a-NSF, blue). (d) The 2D time-resolved emission measurement of coupled-NSs thin-film (100 μJ/cm^2) and representative control sample (here, individual nanospheres dispersed in ethanol). Similar 2D plots were obtained for the coupled-NSs when excited with lower than threshold fluence and for the rapidly annealed sample.

crystalline nanostructures with combined effects of increasing many-body interactions (i.e., carrier−carrier, carrier−phonon). The gain is enhanced by the accumulated in-plane emission scattering while the loss rate is minimized by reducing "voids" in the nanostructured film when the size of the nanospheres is decreased. This strategy allows us to achieve lasing even in films with thickness of ~ $\lambda_{emission}/4$. Overall, this system achieves an order of magnitude reduction in the fluence threshold in films a few orders of magnitude thinner than previously reported.[14,17,18,21] This nanostructured lasing medium has characteristics of both QD-ASE and random lasing insofar that distinct modes are seen transiently in emission, while the low lasing thresholds (<75 μJ/cm^2) enable the excitonic lasing condition, that is, lasing at photoexcited carrier densities below the Mott transition (i.e., exciton to electron−hole plasma).[15,22] Using an ultrafast transient emission method, we quantify the effect of fluence on these many-body interactions that lead to excitonic lasing on the spectral and temporal dynamical evolution of the various lasing modes and on the build-up time of the lasing process.

To fabricate the subwavelength random lasers, we assemble highly crystalline zinc oxide nanospheres[22] with high refractive index (n = 2.3) and strong photoluminescence in the UV into thin films via solution processing methods (Figure 1a, see also Figure S1 in Supporting Information). We observed emission line narrowing and threshold behavior at ~65 μJ/cm^2, above which the emission intensity changes by 3 orders of magnitude (nanosphere film, NSF, Figure 1b,c), indicative of a lasing process. Threshold behavior is always observed in films with thickness greater than 100 nm as measured by scanning electron microscopy and ellipsometry with values for average thickness that are roughly quantized by the number of 35 nm diameter nanostructures in the out-of-plane direction (~105, 140, and 160 nm for 3, 4, and 5, respectively). Threshold behavior was observed over the full range of pump-spot sizes were able to access, from 2.2 μm−1 mm (Figure S2).

To confirm that these emission features are derived from a collective process, we report that no line narrowing or threshold behavior is observed in (i) individual ZnO nanospheres (d-NS for NS dispersed in solution, gray curve in Figure 1b), (ii) samples that had thicknesses less than a 100 nm (i.e., <3 nanospheres thick), or (iii) in any nanosphere-films in which a rapid, high-temperature annealing process was employed (a-NSF, orange curve in Figure 1b,c). Furthermore, we observe drastic changes in the temporal behavior of the emission above threshold in addition to changes in the intensity and emission line shape. Using an ultrafast transient emission technique (Methods, Figure S3), we observe a picosecond time scale emission process that is at least an order of magnitude faster than in an isolated nanostructure or films excited under nonlasing conditions (Figure 1d). Together, these results demonstrate an emission process that is highly sensitive to both geometric (density, size, film morphology) and electronic considerations; while a high density of nanospheres is an imperative requisite for gain, fusing of the nanospheres during this rapid annealing process changes the scattering profile and introduces interfacial trap states that inhibit the lasing action.

While spectral line narrowing, threshold behavior, and fast emission all are highly suggestive of a lasing process, the criteria for proving random lasing necessitate a demonstration of optical gain. To confirm optical gain and understand the gain temporal profile, we use the linear and transient optical absorption spectra. Briefly, for transient absorption measurements a 280 nm ultrafast laser pump pulse (~100 fs) creates a density of electron−hole pairs above the optical bandgap while a weak broadband probe pulse, time-delayed with respect to the pump, monitors the relaxation dynamics of the excited carriers returning to the ground state.[7,23] To highlight the nonlinear

DOI: 10.1021/acs.nanolett.5b05274
Nano Lett. 2016, 16, 2004−2010

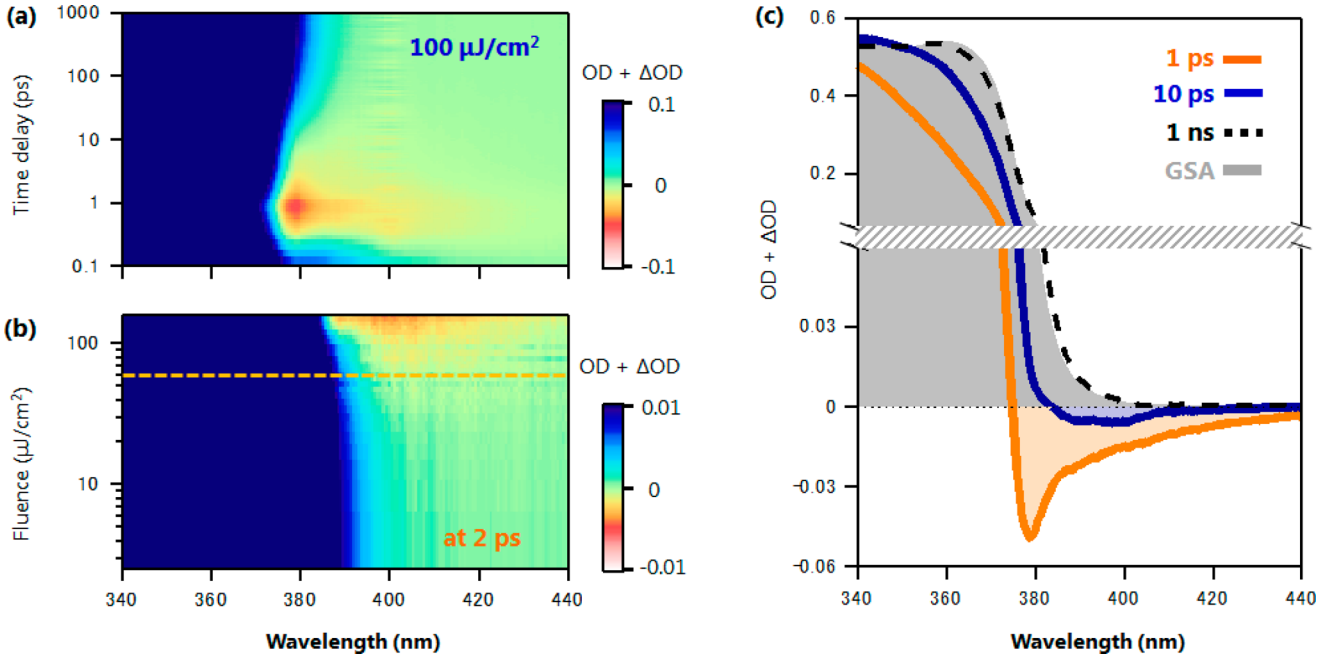

Figure 2. Optical gain in a coupled nanosphere film. (a) The 2D-time-resolved map of the optical gain, obtained by summing the linear and transient optical absorption. (b) Optical gain (OD + ΔOD) at 2 ps after photoexcitation, plotted as a function of pump fluence. Yellow line is only a guide to the eye and represents the region near the fluence threshold. (c) Spectral slices of the optical gain map in (a) at 1 ps, 10 ps, and 1 ns, along with the ground-state linear absorption.

evolution of the system, the raw transient absorption data is processed so that the absolute absorption of the sample, measured using an integrating sphere, is added to each transient spectrum. From this treatment, optical gain can be readily visualized as it corresponds to signals where the OD + ΔOD value is negative.[6,24] A representative 2D data set, displaying OD + ΔOD as a function of time and probe wavelength, is shown in Figure 2a for a pump fluence (100 μJ/cm^2) above the lasing threshold. The ΔA scale is set to highlight the negative signal (optical gain) that develops in the region between 380−420 nm. As in the steady-state emission measurements (Figure 1c), the optical gain signal is nonlinear in the fluence and exhibits a threshold behavior. This can be readily seen in Figure 2b, which shows the transient spectrum at a fixed time (2 ps after excitation) as a function of pump fluence, where the nonlinear component emerges at pump fluences around 60−70 μJ/cm^2 (OD + mOD < 0). A comparison of the linear and transient signals at few critical time delays is shown in Figure 2c. The gain lifetime lasts for less than 10 ps though a small transient signal persists for longer times.

Furthermore, we identify discrete lasing modes in the absence of an external optical cavity, the critical signature of a random lasing mechanism. This is apparent in the slight differences that we observe in the lasing spectra as a function of both sample position and in time (Figure S4). Furthermore, using a high sensitivity transient emission technique based on optical Kerr gating (Figure S3), described previously, we are able to resolve the temporal dynamics of individual modes with ∼200 fs time resolution.[25] By examining spectral slices at discrete times after pumping in a 140 nm thick ZnO−NSs film (Figure S5), we observe that lasing modes are transiently populated as the system evolves. Because they evolve with a distinct time domain behavior, we can clearly see that the individual modes have a line width that is narrower than the time-averaged value. Taken together, these features establish that a random lasing process is occurring. The number of lasing modes and the overall bandwidth increases dramatically with increasing fluence, and on average the red-shifted modes appear at later times that those on the blue edge of the spectrum. This time delay associated with the red-shifted modes is consistent with a shift away from the maximum of the gain curve for ZnO along with decreased scattering efficiency. At higher fluences (>300 μJ/cm^2), more complex spectral dynamics are observed. We note that narrowing of the line width to less than a nanometer is not a necessary signature of random lasing. The observation of relatively broad lasing modes (low Q factor) is consistent with their ultrafast (subps) lifetime. Also, using small nanospheres with a narrow size distribution provides a large number of optimum optical path lengths within the gain bandwidth.

In addition to understanding the mechanism that triggers lasing in those subwavelength assemblies of weakly scattering nanospheres, the ultrafast transient emission measurements allow us to understand differences in the lasing behavior under low and high fluence pump conditions. Below the lasing threshold (29 μJ/cm^2), relatively static emission dynamics are seen with a lifetime of ∼37 ps, similar to isolated nanostructures (Figure 3a). Near threshold (∼60 μJ/cm^2), the first sign of lasing is apparent with "spikes" of intense emission occurring at a few to 100 fs intervals (see arrows in Figures 3b and 4a). These pronounced transient oscillations, or laser spiking, are a direct signature of the scattering mechanism that causes population inversion[13,26] and a direct consequence of the sample trying to reduce the dwell time of the photons in the medium during population inversion.[27]

Under high fluence pumping, the complex lasing dynamics can be explained by the overlapping, ultrafast emission modes and the crossover from excitonic to electron−hole plasma lasing behavior. Just above threshold, the system is in the exciton lasing regime because the optical pump fluence

DOI: 10.1021/acs.nanolett.5b05274
Nano Lett. 2016, 16, 2004−2010

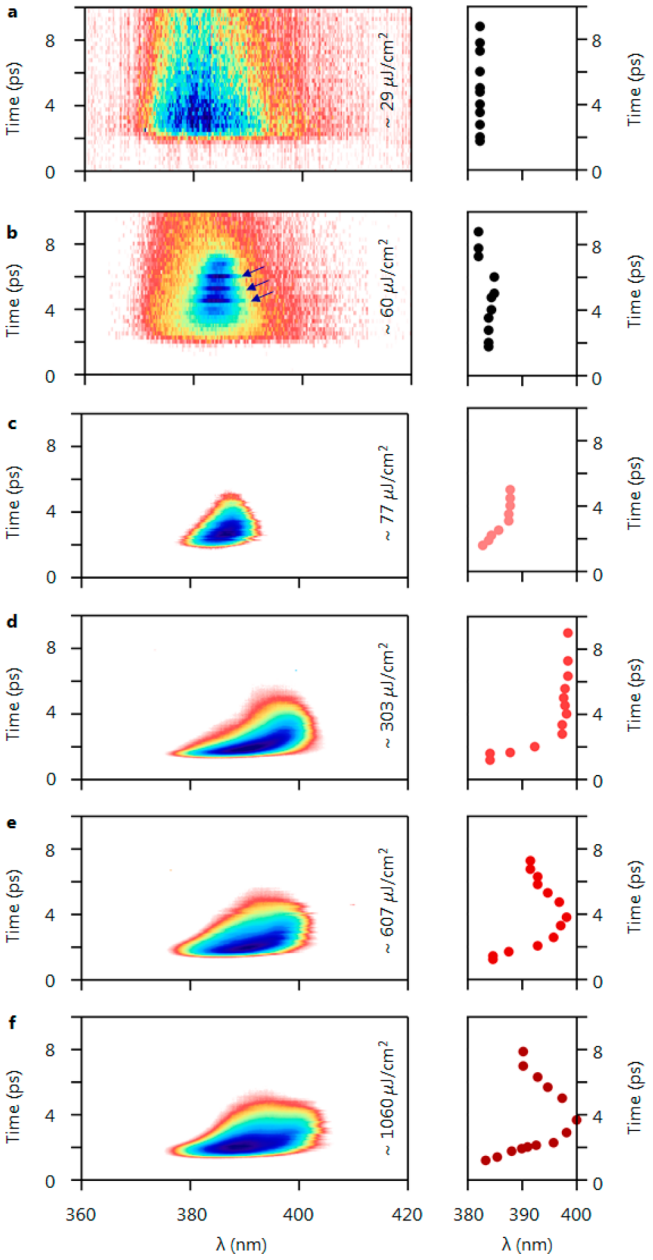

Figure 3. Emission dynamics at low and high fluence. Evolution of the emission spectrum for the pristine-CNF as optical pump fluence is gradually increased from (a) 29 to (f) 1060 $\mu J/cm^2$. The 60 $\mu J/cm^2$ pump fluence data is characteristic of the near-lasing threshold behavior and exhibitd both below and above threshold spectrotemporal features. Figures on the right side track the peak emission intensity with time. Above, 300 $\mu J/cm^2$ signatures the transition from exciton to electron hole plasma lasing can be seen from the dynamics shifting of the emission maxima. Note that emission dynamics in panels a,b and c–f have been gated using the optical Kerr effect in benzene and glass respectively, with a temporal resolution of ~530 and ~220 fs. Note that all 2D TRPL plots have been normalized.

corresponds to carrier densities of $\sim 1.5 \times 10^{18}$ cm^{-3}, much lower than the Mott threshold value ($n_M = k_B T/2a_o^3 E_{exc} \sim 3.7 \times 10^{19}$ cm^{-3}; where a_o is the Bohr's radius of 18 Å and E_{exc} is the exciton binding energy of 60 meV).[15] The spectral dynamics reinforce this conclusion, as an immediate redshift corresponding to P-band exciton scattering is seen in Figure 4c.[28,29] Although such spectral shifts have been reported in steady-state experiments on ZnO microcavities[30] and nanowires,[31] here the dynamic exciton–exciton scattering process is monitored in real time. With increasingly higher fluences, the initial exciton scattering mechanism[32−34] is quickly subdued by the formation of an electron–hole plasma (EHP). The EHP signature is a drastic red shift and broadening in the emission at early times followed by a dynamic blue shift as carriers decay to the ground state and the density drops below the plasma threshold.[35] This behavior is clearly seen by plotting the maxima of the lasing emission wavelength as a function of time (right panels of Figure 3). At higher fluences (Figure 3d–f), the emission maximum is initially red-shifted by 10 nm compared to Figure 3c and exhibits a dynamic recovery of excitonic lasing at 390 nm after a few picoseconds due to the decay of excess carrier density and a return to the excitonic regime.

The dependence of the lasing buildup time on the carrier density, that is, pump fluence, suggests that electron–phonon coupling is important for achieving low-threshold lasing. After precisely determining time zero based on the arrival time of the excitation pulse, we plot the kinetics of the system at the emission maximum (Figure 4a,b) and the buildup time (Figure 4c) for different pump fluences. Notably, the maximum delay of ~2.5 ps occurs precisely at the lasing fluence threshold. The change in buildup time highlights the complicated interaction between excited carriers and the phonon modes that exist in the gain material and which have been shown to be crucial for lasing in II–VI semiconductors[36] in the low fluence regime.[37] Moreover, this delay highlights the importance of phonon modes in distributing excitons within the continuum states,[31,38,39] thus reducing intraband nonradiative exciton–exciton scattering and ultimately fulfilling the population inversion that initially triggers lasing. With an increased density of excited carriers, additional carrier–carrier scattering into the continuum states[40] occurs and the temporal delay in lasing is reduced.

Additional insight into the mechanism of exciton random lasing in the subwavelength limit is obtained using full-field 3D electromagnetic simulations (see details in Methods section), which confirm that lasing is seeded from the collective scattering of the nanospheres. These simulations explored the effect of film morphology and disorder on the ability to localize and enhance the electromagnetic field over the relevant spectral range (350–450 nm). In Figure 5, we plot the electric field enhancement, $|E|^2$, at the emission peak (~403 nm) in a 140 nm thin film composed of unstructured ZnO, a close-packed film composed of ZnO nanospheres with diameter of 40 nm, and a film of randomly arranged ZnO nanospheres with a distribution of diameters between 40 and 50 nm. Significant enhancement near the ZnO bandedge emission occurs only for the film composed of randomly packed, heterogeneous ZnO nanospheres. Identically thick films of unstructured and well-aligned close-packed ZnO do not show a similar dramatic increase in scattering at any relevant wavelength. These results show that the randomly arranged nanospheres are required to confine the light fields within the film and to consequently increase the in-plane scattering needed to achieve lasing.

From the combined spectrotemporal dynamics and electromagnetic simulations, we build a mechanistic picture of how low-threshold random lasing occurs in these thin-films composed of nanospheres that individually display weak scattering properties. The subdiffraction length scales serve to confine the incoming light fields within the bifunctional gain media and selectively outcompete extended modes that allow

DOI: 10.1021/acs.nanolett.5b05274
Nano Lett. 2016, 16, 2004–2010

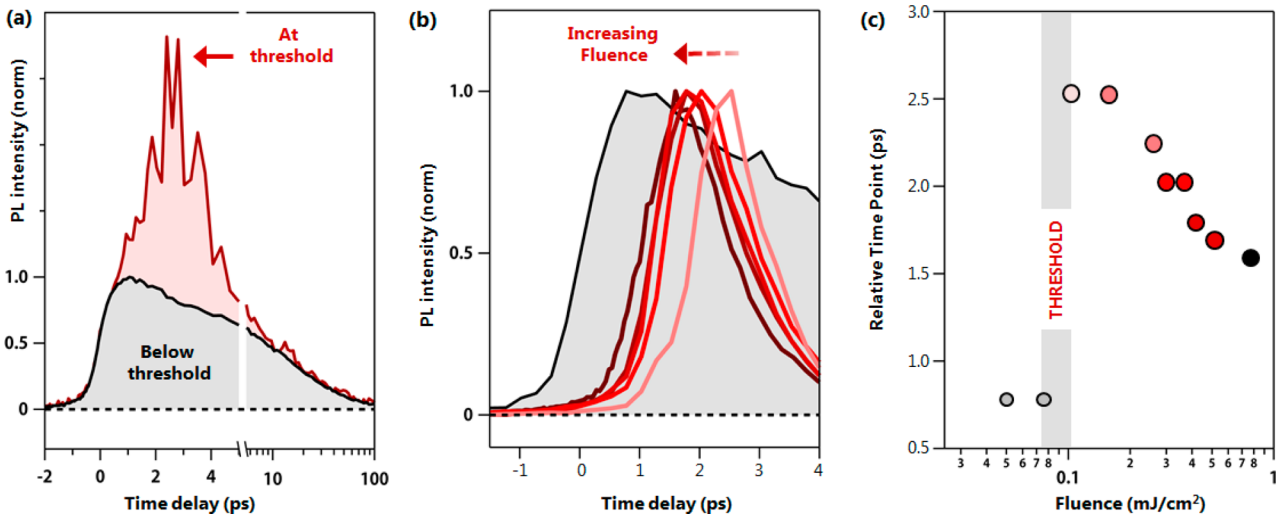

Figure 4. Fluence-dependent buildup time on lasing. (a) Kinetic traces at band-edge emission of thin-film coupled nanospheres below and at near-lasing threshold. At threshold, lasing instabilities can be seen superimposed on the normal fluorescence decay during the first few picoseconds. (b) Kinetics traces for various pump fluences above lasing threshold and (c) the time delay of the emission maximum relative to the pump pulse arrival time as a function of pump fluence.

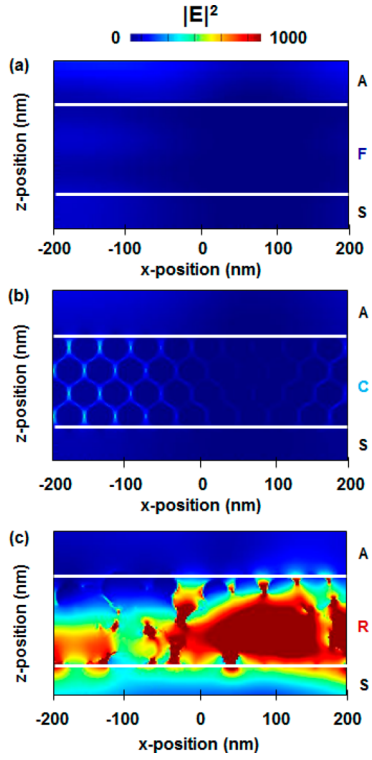

Figure 5. Near-field electromagnetic distributions of various ZnO thin-film configurations. *XZ*-plane comparing the $|E|^2$ at the emission peak (~403 nm) for (a) flat, unstructured thin-film, (b) close-packed film composed of ZnO nanospheres with diameter of 40 nm and (c) randomly arranged ZnO nanospheres with a uniform size distribution, ranging between 40 and 50 nm in diameter. Enhancement in the in-plane emission scattering is clearly visible only for the case when the film is composed of the random nanospheres. For ease of comparison, all plots share the same color scale. A, air; S, substrate; F, flat-film; C, close-packed film; R, randomly packed film.

the emitted photons to diffuse throughout micron-thick samples.[13,17,26] In addition, the smaller nanospheres reduce the voids, providing a closer packing capacity (greater gain-to-volume fraction). Consequently, this increases coherent particle-particle and photon-particle scattering processes while accelerating their decay via amplified stimulated emission. To estimate the magnitude of this effect, we can assume a certain packing arrangement (see Supporting Information, Figure S6) and compute the gain-to-void fraction as the particle size is changed. We see that decreasing the nanospheres diameter from 200 to 35 nm results in a drastic decrease of the void feature size by about 90%.

In conclusion, we have demonstrated low-threshold excitonic UV-blue lasing (<75 $\mu J/cm^2$) in an ultrathin-film of coupled nanospheres. Resolving the subpicosecond absorption and emission dynamics below and above threshold provide insights into the material requirements for lasing in disordered materials. For example, we show that the gain mechanism is excitonic random lasing via multiple in-plane scattering, despite the use of weakly scattering 35 nm diameter nanostructures and subwavelength film thicknesses. Our results suggest that coupled, highly crystalline nanostructures, fabricated by low-cost solution processing methods, can function as viable building blocks for high-performance optoelectronic devices.

Methods. *Fabrication of ZnO Nanospheres Sample.* Hydrothermally grown ZnO nanostructures that are dispersed in ethanol with an average size of ~35 nm and 40% weight concentration (~10% volume concentration) were obtained from Sigma-Aldrich. This solution was further diluted to 0.7% volume concentration and spun-cast at 10 000 rpm for 60 s and baked at 300 °C for 10 min to remove the residual ethanol solvent. To vary the sample thickness, a different concentration of the dispersed solution was used. The resulting spin-coated nanostructures formed a close-packed thin film as shown in the scanning electron micrograph of Figure 1a. The thicknesses of the films were estimated using ellipsometric techniques and scanning electron microscopy.[41] As controls, (i) similar spin-coated samples with varying thickness were annealed for a short duration using a rapid thermal process (RTP conditions: 5 minutes at 800 °C), and for dispersed nanosphere studies (ii) the initial solution used was placed in a 1 mm cuvette for time-resolved emission studies.

DOI: 10.1021/acs.nanolett.5b05274
Nano Lett. 2016, 16, 2004−2010

Optical Characterization. For all optical spectroscopy measurements (steady-state emission and ultrafast transient and emission measurements), an excitation pulse of wavelength 280 nm, pulse duration of 100 fs, and focus to a spot size of about 500 μm in diameter was used (pump). The experiments were conducted using a Ti:sapphire laser system (Spectra Physics) with the pump being generated using a commercial optical parametric amplifier (OPA, Light Conversion Ltd.). For transient absorption measurements, a supercontinuum probe was generated by focusing the 800 nm fundamental light into a calcium fluoride plate. Shot-by-shot detection was achieved using fast silicon multichannel detectors (Ultrafast Systems LLC). For ultrafast transient emission experiments, a high-sensitivity home-built setup based on the optical Kerr effect was used.[25] The modularity of our setup allows low emissive states to be gated/probed using benzene as the Kerr medium[22,42] in the low fluence limit with a temporal resolution of ~530 fs and quartz in the high fluence limit with a time resolution of ~220 fs. The gated emission signal is collimated and hereafter focused onto an imaging, nitrogen-cooled spectrometer (iHR320), equipped with a charge-coupled camera (SymphonyII, HORIBA Jobin Yvon). More details are also presented in the Supporting Information.

Electromagnetic Simulations. To confirm the effect of a random assembly of nanostructures on its in-plane emission scattering, we use full-field 3D finite-difference time-domain software (Lumerical Solutions) to calculate the near-field electromagnetic distributions in a variety of films with a constant thickness of 140 nm. The volume simulated was 500 × 500 × 700 nm^3 with x and y having periodic boundary conditions while z had a perfect matching layer (parameters were 24 layers, $\kappa = 2$ and $\sigma = 0.25$). A set of dipole emitters (arranged to simulate random polarization and in the spectral range 350−450 nm) was placed in the simulation volume while XZ-plane monitors were placed at the center of the simulated volume, that is, $y = 0$, to record the transmission and electromagnetic near-field distributions of the system. In all cases, these parameters were kept constant with only the film morphology being varied. Simulations were performed on a (i) flat and unstructured, (ii) close-packed nanosphere and (iii) randomly distributed nanosphere thin-film. For the random nanostructures, we use the uniform randomly distributed nanophere function with diameter parameter set to range around 40 nm. The same ZnO dielectric value was used for all configurations.

■ ASSOCIATED CONTENT

Supporting Information

The Supporting Information is available free of charge on the ACS Publications website at DOI: 10.1021/acs.nanolett.5b05274.

Scanning electron microscopy images of nanosphere films, excitation spot size measurements, additional experimental details, position and temporal variations of lasing spectra, evidence of discrete lasing modes, and calculation of void sizes as a function of nanosphere size and film thickness. (PDF)

■ AUTHOR INFORMATION

Corresponding Author

*E-mail: msfeir@bnl.gov.

Author Contributions

X.L., V.M., K.A., and M.Y.S. designed the experiment. X.L. fabricated the samples. K.A. and X.L. collected and K.A. and M.Y.S. analyzed the ultrafast measurements. All authors interpreted the results and contributed to writing the manuscript.

Funding

This research used resources of the Center for Functional Nanomaterials, which is a U.S. DOE Office of Science User Facility, at Brookhaven National Laboratory under Contract No. DE-SC0012704. Work at the City College of New York is supported by the National Science Foundation through Grant DMR 1410249.

Notes

The authors declare no competing financial interest.

■ ACKNOWLEDGMENTS

The authors thank Erik Busby and Dmytro Nykypanchuk for helpful discussions.

■ REFERENCES

(1) Dang, C.; Lee, J.; Breen, C.; Steckel, J. S.; Coe-Sullivan, S.; Nurmikko, A. Red, Green and Blue Lasing Enabled by Single-Exciton Gain in Colloidal Quantum Dot Films. *Nat. Nanotechnol.* **2012**, *7*, 335−339.

(2) Feng, L.; Wong, Z. J.; Ma, R.-M.; Wang, Y.; Zhang, X. Single-Mode Laser by Parity-Time Symmetry Breaking. *Science* **2014**, *346*, 972−975.

(3) Ma, R.-M.; Oulton, R. F.; Sorger, V. J.; Bartal, G.; Zhang, X. Room-Temperature Sub-Diffraction-Limited Plasmon Laser by Total Internal Reflection. *Nat. Mater.* **2011**, *10*, 110−113.

(4) Cooney, R. R.; Sewall, S. L.; Sagar, D. M.; Kambhampati, P. Gain Control in Semiconductor Quantum Dots Via State-Resolved Optical Pumping. *Phys. Rev. Lett.* **2009**, *102*, 127404.

(5) Ivanov, S. A.; Achermann, M. Spectral and Dynamic Properties of Excitons and Biexcitons in Type-Ii Semiconductor Nanocrystals. *ACS Nano* **2010**, *4*, 5994−6000.

(6) Sewall, S. L.; Franceschetti, A.; Cooney, R. R.; Zunger, A.; Kambhampati, P. Direct Observation of the Structure of Band-Edge Biexcitons in Colloidal Semiconductor Cdse Quantum Dots. *Phys. Rev. B: Condens. Matter Mater. Phys.* **2009**, *80*, 081310.

(7) Cooney, R. R.; Sewall, S. L.; Sagar, D. M.; Kambhampati, P. State-Resolved Manipulations of Optical Gain in Semiconductor Quantum Dots: Size Universality, Gain Tailoring, and Surface Effects. *J. Chem. Phys.* **2009**, *131*, 164706.

(8) Klimov, V. I.; Ivanov, S. A.; Nanda, J.; Achermann, M.; Bezel, I.; McGuire, J. A.; Piryatinski, A. Single-Exciton Optical Gain in Semiconductor Nanocrystals. *Nature* **2007**, *447*, 441−446.

(9) Moreels, I.; Rainò, G.; Gomes, R.; Hens, Z.; Stöferle, T.; Mahrt, R. F. Nearly Temperature-Independent Threshold for Amplified Spontaneous Emission in Colloidal Cdse/Cds Quantum Dot-in-Rods. *Adv. Mater.* **2012**, *24*, OP231−OP235.

(10) Guzelturk, B.; Kelestemur, Y.; Olutas, M.; Delikanli, S.; Demir, H. V. Amplified Spontaneous Emission and Lasing in Colloidal Nanoplatelets. *ACS Nano* **2014**, *8*, 6599−6605.

(11) Cirloganu, C. M.; Padilha, L. A.; Lin, Q.; Makarov, N. S.; Velizhanin, K. A.; Luo, H.; Robel, I.; Pietryga, J. M.; Klimov, V. I. Enhanced Carrier Multiplication in Engineered Quasi-Type-II Quantum Dots. *Nat. Commun.* **2014**, *5*, 4148.

(12) Wang, J.; Genack, A. Z. Transport through Modes in Random Media. *Nature* **2011**, *471*, 345−348.

(13) Wiersma, D. S.; Lagendijk, A. Light Diffusion with Gain and Random Lasers. *Phys. Rev. E: Stat. Phys., Plasmas, Fluids, Relat. Interdiscip. Top.* **1996**, *54*, 4256−4265.

DOI: 10.1021/acs.nanolett.5b05274
Nano Lett. 2016, 16, 2004−2010

(14) Cao, H.; Zhao, Y. G.; Ho, S. T.; Seelig, E. W.; Wang, Q. H.; Chang, R. P. H. Random Laser Action in Semiconductor Powder. *Phys. Rev. Lett.* **1999**, *82*, 2278−2281.
(15) Klingshirn, C.; Fallert, J.; Zhou, H.; Sartor, J.; Thiele, C.; Maier-Flaig, F.; Schneider, D.; Kalt, H. 65 Years of Zno Research − Old and Very Recent Results. *Phys. Status Solidi B* **2010**, *247*, 1424−1447.
(16) Nakamura, T.; Firdaus, K.; Adachi, S. Electron-Hole Plasma Lasing in a Zno Random Laser. *Phys. Rev. B: Condens. Matter Mater. Phys.* **2012**, *86*, 205103.
(17) Fallert, J.; Dietz, R. J. B.; Sartor, J.; Schneider, D.; Klingshirn, C.; Kalt, H. Co-Existence of Strongly and Weakly Localized Random Laser Modes. *Nat. Photonics* **2009**, *3*, 279−282.
(18) Nakamura, T.; Fujiwara, H.; Niyuki, R.; Sasaki, K.; Ishikawa, Y.; Koshizaki, N.; Tsuji, T.; Adachi, S. Origins of Lasing Emission in a Resonance-Controlled Zno Random Laser. *New J. Phys.* **2014**, *16*, 093054.
(19) Apalkov, V. M.; Raikh, M. E.; Shapiro, B. Random Resonators and Prelocalized Modes in Disordered Dielectric Films. *Phys. Rev. Lett.* **2002**, *89*, 016802.
(20) Fujiwara, H.; Hamabata, Y.; Sasaki, K. Numerical Analysis of Resonant and Lasing Properties at a Defect Region within a Random Structure. *Opt. Express* **2009**, *17*, 3970−3977.
(21) Xing, G.; Xing, G.; Li, M.; Sie, E. J.; Wang, D.; Sulistio, A.; Ye, Q.-l.; Huan, C. H. A.; Wu, T.; Sum, T. C. Charge Transfer Dynamics in Cu-Doped Zno Nanowires. *Appl. Phys. Lett.* **2011**, *98*, 102105−3.
(22) Appavoo, K.; Liu, M.; Sfeir, M. Y. Role of Size and Defects in Ultrafast Broadband Emission Dynamics of Zno Nanostructures. *Appl. Phys. Lett.* **2014**, *104*, 133101.
(23) Almand-Hunter, A. E.; Li, H.; Cundiff, S. T.; Mootz, M.; Kira, M.; Koch, S. W. Quantum Droplets of Electrons and Holes. *Nature* **2014**, *506*, 471−475.
(24) Busby, E.; Thibert, A.; Fuzell, J.; Arrington, D. C.; Jawaid, A. M.; Snee, P. T.; Larsen, D. S. Ultrafast Exciton Dynamics in Colloidal Aluminum Phosphide Nanocrystals. *Chem. Phys. Lett.* **2013**, *557*, 129−133.
(25) Appavoo, K.; Sfeir, M. Y. Enhanced Broadband Ultrafast Detection of Ultraviolet Emission Using Optical Kerr Gating. *Rev. Sci. Instrum.* **2014**, *85*, 055114.
(26) Berger, G. A.; Kempe, M.; Genack, A. Z. Dynamics of Stimulated Emission from Random Media. *Phys. Rev. E: Stat. Phys., Plasmas, Fluids, Relat. Interdiscip. Top.* **1997**, *56*, 6118−6122.
(27) Siegman, A. E. *Lasers*; University Science Books: Sausalito, CA, 1986.
(28) Guillaume, C. B.; Debever, J.-M.; Salvan, F. Radiative Recombination in Highly Excited Cds. *Phys. Rev.* **1969**, *177*, 567−580.
(29) Hönerlage, B.; Klingshirn, C.; Grun, J. B. Spontaneous Emission Due to Exciton-Electron Scattering in Semiconductors. *Phys. Status Solidi B* **1976**, *78*, 599−608.
(30) Guillet, T.; Brimont, C.; Valvin, P.; Gil, B.; Bretagnon, T.; Médard, F.; Mihailovic, M.; Zúñiga-Pérez, J.; Leroux, M.; Semond, F.; et al. Laser Emission with Excitonic Gain in a Zno Planar Microcavity. *Appl. Phys. Lett.* **2011**, *98*, 211105.
(31) Zimmler, M. A.; Capasso, F.; Müller, S.; Ronning, C. Optically Pumped Nanowire Lasers: Invited Review. *Semicond. Sci. Technol.* **2010**, *25*, 024001.
(32) Yamamoto, A.; Kido, T.; Goto, T.; Chen, Y.; Yao, T.; Kasuya, A. Dynamics of Photoexcited Carriers in Zno Epitaxial Thin Films. *Appl. Phys. Lett.* **1999**, *75*, 469−471.
(33) Bauer, C.; Boschloo, G.; Mukhtar, E.; Hagfeldt, A. Ultrafast Relaxation Dynamics of Charge Carriers Relaxation in Zno Nanocrystalline Thin Films. *Chem. Phys. Lett.* **2004**, *387*, 176−181.
(34) Mehl, B. P.; Kirschbrown, J. R.; Gabriel, M. M.; House, R. L.; Papanikolas, J. M. Pump−Probe Microscopy: Spatially Resolved Carrier Dynamics in Zno Rods and the Influence of Optical Cavity Resonator Modes. *J. Phys. Chem. B* **2013**, *117*, 4390−4398.
(35) Toshine, Y.; Takeda, J.; Ko, H. J.; Yao, T. Conversion of an Electron−Hole Plasma into a High Density Excitonic State in Zno Epitaxial Thin Films. *Phys. Status Solidi C* **2004**, *1*, 839−842.
(36) Haug, H.; Grob, K. Exciton Laser Theory. *Phys. Lett. A* **1967**, *26*, 41−42.
(37) Haug, H. Theory of Laser Action Involving Free Excitons and Lo-Phonon-Assisted Transitions. *J. Appl. Phys.* **1968**, *39*, 4687−4695.
(38) Hendry, E.; Koeberg, M.; Bonn, M. Exciton and Electron-Hole Plasma Formation Dynamics in Zno. *Phys. Rev. B: Condens. Matter Mater. Phys.* **2007**, *76*, 045214.
(39) Versteegh, M. A. M.; Kuis, T.; Stoof, H. T. C.; Dijkhuis, J. I. Ultrafast Screening and Carrier Dynamics in Zno: Theory and Experiment. *Phys. Rev. B: Condens. Matter Mater. Phys.* **2011**, *84*, 035207.
(40) Zhang, X. H.; Chua, S. J.; Yong, A. M.; Yang, H. Y.; Lau, S. P.; Yu, S. F.; Sun, X. W.; Miao, L.; Tanemura, M.; Tanemura, S. Exciton Radiative Lifetime in Zno Nanorods Fabricated by Vapor Phase Transport Method. *Appl. Phys. Lett.* **2007**, *90*, 013107.
(41) Liu, X.; Goldberg, D.; Menon, V. M. Formation of Microcavity Polaritons in Zno Nanoparticles. *Opt. Express* **2013**, *21*, 20620−20625.
(42) Appavoo, K.; Liu, M.; Black, C. T.; Sfeir, M. Y. Quantifying Bulk and Surface Recombination Processes in Nanostructured Water Splitting Photocatalysts Via in Situ Ultrafast Spectroscopy. *Nano Lett.* **2015**, *15*, 1076−1082.

DOI: 10.1021/acs.nanolett.5b05274
Nano Lett. 2016, 16, 2004−2010